Doped SnO 2 thin films fabricated at low temperature by atomic layer deposition with a precise incorporation of niobium atoms

Getaneh Diress Gesesse, Damien Coutancier, Mirella Al Katrib, Frédérique Donsanti, Muriel Bouttemy, Nathanaelle Schneider

Doped SnO_2 thin films fabricated at low temperature by atomic layer deposition with a precise incorporation of niobium atoms

Getaneh Diress Gesesse[1], Damien Coutancier[1,2], Mirella Al Katrib[1,3], Frédérique Donsanti[1,4], Muriel Bouttemy[1,3], Nathanaelle Schneider[1,2*]

[1] Institut Photovoltaïque d'Ile-de-France (IPVF), 18 Boulevard Thomas Gobert, 91120 Palaiseau, France
[2] UMR-IPVF 9006, CNRS, Institut Photovoltaïque d'Ile-de-France (IPVF), 18 Boulevard Thomas Gobert, 91120 Palaiseau, France
[3] UMR 8180, CNRS, Institut Lavoisier de Versailles (ILV), Université de Versailles Saint-Quentin-en-Yvelines (UVSQ), 45 avenue des Etats-Unis, 78035 Versailles, France
[4] EDF R&D, Institut Photovoltaïque d'Ile-de-France (IPVF), 18 Boulevard Thomas Gobert, 91120 Palaiseau, France

*E-mail: n.schneider@cnrs.fr

Received xxxxxx

Accepted for publication xxxxxx
Published xxxxxx

Abstract

Nb-doped SnO_2 (NTO) thin films were synthesized by atomic layer deposition technique at low temperature (100 °C). For an efficient incorporation of the Nb atoms, i.e. fine control of their amount and distribution, various supercycle ratios and precursor pulse sequences were explored. The thin film growth process studied by in-situ QCM revealed that the Nb incorporation is highly impacted by the surface nature as well as the amount of species available at the surface. This was confirmed by the actual concentration of the Nb atom incorporated inside the thin film as determined by XPS. Highly transparent thin films which transmit more than 95% of the AM1.5 global solar irradiance over a wide spectral range (300-1000 nm) were obtained. In addition, the Nb atoms influenced the optical band gap, conduction band, and valence band levels. While SnO_2 thin film were too resistive, films tuned to conductive nature upon Nb incorporation with controlled concentration. Optimal incorporation level was found to be $\leq$1 at.% of Nb, and carrier concentration reached up $2.5x10^{18}/cm^3$ for the as-deposited thin films. As a result, the high optical transparency accompanied with tuned electrical property of NTO thin films fabricated by ALD at low temperature paves the way for their integration into temperature-sensitive, nanostructured optoelectrical devices.

Keywords: doped SnO_2 thin films, Nb incorporation, ALD, supercycle, pulse sequence

1. Introduction

Tin oxide (SnO_2) is an n-type semiconductor with a direct band gap energy of 3.6 eV that has been efficiently used in various optoelectronic, photovoltaic, and energy storage devices [1]. Pure SnO_2 thin films often suffer from low electrical conductivity caused by inadequate concentration of oxygen vacancies,[2,3] which is mainly dependent from the synthesis methods. The electrical properties of SnO_2 thin films can be improved by incorporating various doping elements, such as F, Sb, Nb, W, Ta, Mo, Li, Co, and Ga [1,4]. For an efficient n-doping, the incorporated ion must have a higher number of valence electrons than the host atom, as well as close ionic radius to make easier the distribution of the ion in the lattice structure of the host atom [5]. Accordingly, among the potential SnO_2 doping elements, Nb ($[Kr]4d^45s^1$) with ionic radius of 0.64Å (Nb^{+V}) is a very promising candidate to be incorporated with Sn ($[Kr]4d^{10}5s^25p^2$) having ionic radius of 0.69Å (Sn^{+IV}) [6]. This is supported by theoretical calculations on the electronic structure of Nb incorporated SnO_2 that report higher density of states at the Fermi level leading to its metallic type of conductivity, than with other potential dopants, [7].

In this context, Nb incorporated SnO_2 (NTO) films have been investigated by different deposition methods such as chemical bath deposition [8], pulsed laser deposition [9], metal-organic chemical vapor deposition [10], atomic layer deposition [11], sputtering [12], spin-coating [13], spray-pyrolysis [14], and dip-coating [15] for various applications. These reports experimentally confirmed that the incorporation of Nb atom modifies the electrical and optical properties of SnO_2 films. Also, they emphasized that the Nb atom concentration needs to be controlled, optimized, and kept below 5% in most cases. However, most of these fabrication methods usually suffer from non-uniformity, non-conformality [16], and require post-deposition annealing treatment.

For a fine tuning of element incorporation and successful integration of thin films into devices, atomic layer deposition (ALD) has clear advantages over other deposition techniques. Based on self-limited surface chemical reactions, it leads to ultra-thin films with excellent conformality and uniformity, precise control of thickness at atomic scale and composition even at low temperature [17–19]. Nb atoms have been successfully incorporated to various oxide thin films by ALD such as in TiO_2 [20], ZnO [21], Ta_2O_5 [22], and Al_2O_3 [23]. As for SnO_2, other doping elements such as Al [24] and Ta [25] were also incorporated by ALD. ALD fabricated NTO films were reported by Stefik *et al.* in 2012 that applied in host−guest photoelectrochemical [11] and dye-sensitized solar cell [26] applications. The authors claimed that the presence of Nb atoms efficiently enhances the electrical properties of SnO_2, while the film was 100 nm thick and annealed at 500 °C. These two conditions (thickness, post-annealing) severely limit the applicability of ALD-NTO thin films. Despite the potential of ALD-NTO thin films, to the best of our knowledge, these limitations have not been leveraged since then. Hence, we decided to investigate further the ALD process of NTO thin films and take full benefit from ALD options.

This work aims to access SnO_2 thin films with tuned electrical properties at low temperature (100 °C). For that, ALD process was chosen and Nb atoms were incorporated in SnO_2 thin films without any post-treatments. Such process is adapted for a device that requires finely tuned functional thin films produced at low deposition temperature without post-deposition annealing treatment. A classical method to incorporate atom in ALD process is the *supercycle* approach [27], *i.e.* inserting of a cycle of the doping atom between the host semiconductor cycles, in our case Nb_2O_5 cycle between SnO_2 cycles. The concentration of the incorporated atom can be controlled by varying the cycle ratios between the host semiconductor and the incorporated element. However, these incorporated atoms do not directly translate into doping atoms. Indeed, other factors such as atom distribution are key to ensure efficient doping and additional strategies are required. In particular, the variation of precursor nature [28] and precursor pulse sequences [29–31] have shown an important influence on the growth mechanism and the properties of thin films by enhancing the distribution of incorporated atoms and prevent the formation of nanolaminate or biphasic systems. We sought a comprehensive analysis to understand the influence of the ALD processes (cycle ratio and precursor pulse sequences) on the growth mechanism and how it affects the thin film properties, by *in-situ* and *ex-situ* characterization.

2. Experimental section

2.1 Fabrication of thin films

The NTO thin films were synthesized by thermal ALD technique using a BENEQ TFS-200 ALD reactor, where the deposition temperature (T_{dep}) was maintained at 100 °C and the pressure was at 1.1 mbar. Tetrakis(dimethylamido)tin(IV) ($(((CH_3)_2N)_4Sn$, TDMASn, 99.99% purity, STREM) and tris(diethylamido)(tert-butylimido)niobium(V) ($(((CH_3CH_2)_2N)_3Nb{=}NC(CH_3)_3$, TBTDEN, min. 98% purity, STREM) were used as a precursor of Sn and Nb, respectively. Hydrogen peroxide (H_2O_2, 30% w/w in H_2O) was used as a reactant with Sn precursor while deionized water (H_2O) was used as a reactant with Nb precursor. All chemicals were used without any further purification. TDMASn and TBTDEN were heated in hot solid sources system of Beneq HS 300 at T_{TDMASn} = 60 °C and T_{TBTDEN} = 70 °C, respectively, while the reactants were kept at room temperature. Nitrogen gas (N_2, 99.9999%, Air Liquide) was used as carrier gas and for purge at flow rate of 600 sccm. Films were deposited simultaneously

on various substrates: single-polished n-doped Si (100) wafers with native oxide layer on top, borosilicate glass (5x5 cm^2), soda-lime glass (2x2 cm^2), ITO (2x2 cm^2), and FTO (2x2 cm^2), aimed for various characterizations. Prior to deposition, the borosilicate and soda-lime glasses, ITO, and FTO substrates were cleaned by ultrasonication in acetone and isopropanol during 15 min of each.

The incorporation of Nb were carried out by a *supercycle* approach, which is inserting of a single Nb_2O_5 cycle between SnO_2 cycles with a general program of: NTO = x*(x1.{SnO_2}+{Nb_2O_5}), where x is the number of supercycle and x1 is the number of SnO_2 cycles in one supercycle. Thus, the x1 values were varied as 1, 5, 10, 15, 20, and 55, so the cycle ratio of (SnO_2:Nb_2O_5) is referred as (x1:1). Two precursor/reactant sequences of (i) TDMASn pulse/H_2O_2 pulse/TBTDEN pulse/H_2O pulse (named as SONO) and (ii) H_2O_2 pulse/TDMASn pulse/TBTDEN pulse/H_2O pulse (named as OSNO) with N_2 purge after each pulse were investigated. For betted comparison of films, each deposition was finished with 3 cycles of SnO_2. The fabricated thin films are labelled by combining the sequence and the cycle ratio as SONO(x1:1) or OSNO(x1:1). Pure SnO_2 and Nb_2O_5 thin films were also produced separately. To ensure the proper transport of the metal precursors into the reactor, a combination mode composed of four steps ($t_1/t_2/t_3/t_4$) were used. First, N_2 gas was injected into a precursor source (t_1), then all the valves were closed (t_2), followed by pulsing of the precursor (t_3), and simultaneous N_2 injection with precursor pulse (t_4). The recipe of {SnO_2} corresponds to {(TDMASn pulse)/N_2 purge/H_2O_2 pulse/N_2 purge = (1/0.1/0.5/0.5)/3/1/3 s}, and of {Nb_2O_5} corresponds to {(TBTDEN pulse)/N_2 purge/H_2O pulse/N_2 purge = (1.5/0.05/0.5/2)/5/1/5 s}.

2.2 In-situ ALD growth study

The thin film growth was studied by *in-situ* Quartz Crystal Microbalance (QCM) with a Colnatec Eon-LT monitor system using an HT quartz crystal (6 MHz initial oscillation frequency) located on the cover lid of the ALD reactor. The signal was collected every 0.1 s, and the lowest thickness precision was 0.04 Å. In order to consider the larger reactor volume in QCM configuration and to assure an effective saturation state, longer pulse and purge times than the ones used for thin film fabrication process were used. Growth of SnO_2, Nb_2O_5, SONO(10:1), and OSNO(10:1) thin films were recorded, and the signal averaged over 10 cycles. The conversion of the signal to mass variation was made using impedance acoustic value of Z_f = 1.00 and density of 6.95 g/cm^3 for SnO_2, and Z_f = 1.00 and density of 4.47 g/cm^3 for Nb_2O_5, as input parameters.

2.3 Characterization of thin films

All the characterizations were carried out on the as-deposited thin films. The properties of NTO thin films were characterized by various techniques for samples deposited on single-polished n-doped Si (100) wafers with native oxide layer on top (ellipsometry, XRR, GIXRD, SEM, XPS), borosilicate glass (spectrophotometry), soda-lime glass (Hall effect), ITO (Kelvin probe), and FTO (cyclic voltammetry). Thickness was determined by spectroscopic ellipsometry (SE) using a Horiba Jobin Yvon Uvisel 2 ellipsometer. The SE measurement was performed at incidence angle of 70° in energy range between 1.5 and 5.0 eV with step of 0.05 eV, and the data were fitted using DeltaPsi2 software modelled with Tauc-Lorentz oscillators functions. X-ray reflectivity (XRR) measurement, using PANalytical Empyrean equipment with Cu Kα radiation source (λ=0.15418 nm) operated at 45 kV and 40 mA, was performed for further determination of the thickness, the roughness, and the density of fabricated thin films. The structure was analyzed by grazing incidence X-ray diffraction (GIXRD) using the same PANalytical Empyrean equipment. The surface morphology of thin films was observed using a Merlin VP Compact scanning electron microscope (SEM).

The surface and in-depth chemical compositions were analyzed using X-ray photoelectron spectroscopy (XPS) with Thermo Electron^{TM} k-Alpha$^+$ spectrometer equipped with a monochromatic Al-Kα X-ray source (hv=1486.6 eV). The spectrometer was calibrated using Cu and Au samples following the ASTM-E-902-94 protocol. A X-ray beam diameter of 400 µm was used for both surface points and depth profiles. The survey scans (0-1350 eV) were collected at a pass energy of 100 eV with a step size of 1 eV. High-resolution spectra were measured at a pass energy of 20 eV with a step size of 0.1 eV. An energy calibration was realized with respect to the C 1s peak at 284.8eV. In-depth profile was carried out using a monatomic ion gun (Ar^+) with energy of 1000 eV, current density of 10 mA, ion gun orientation of 30°, and raster width of 2 mm. Avantage Software was employed for quantification and atomic ratios were determined without peaks fitting, only based on the peak area (shirley background subtraction) and the RSF (relative sensitivity factor) of each element. Moreover, angle-resolved XPS (ARXPS) measurement was performed to finely determine the chemistry at the surface and sub-surface by tilting the samples from 0° with respect to the analyzer (i.e. normal incidence) to 60° (to become more surface sensitive).

Transmittance and reflectance spectra were collected using an Agilent Cary 5000 UV-Vis-NIR spectrophotometer equipped with a diffuse reflectance accessory. Work function of thin films was analyzed by a macroscopic Kelvin Probe system using the Besocke Delta Phi: Kelvin Control 07 and Kelvin Probe S (gold tip) instruments. The contact potential difference between the gold tip and the thin films were measured, and the work function of thin films was determined relative to a reference electrode of highly oriented pyrolytic graphite (work function = 4.60 eV). Electrical properties were

studied by Hall effect measurement using ECOPIA HMS-5000 system with a 0.556T permanent magnet at room temperature. Furthermore, the electrochemical response of thin films was studied by cyclic voltammetry in three electrode set-up of reference electrode (Ag/AgCl, 3 M KCl), counter electrode (Pt wire), and working electrode (ALD fabricated thin films on FTO). The electrolyte involves a solution of potassium hexacyanoferrate(III), $K_3[Fe(CN)_6]$, (0.1 mol L^{-1}), and potassium hexacyanoferrate(II), $K_4[Fe(CN)_6]$, (0.1 mol L^{-1}). The current response of each thin film was collected under dark conditions in the potential range of -1.0 V and +1.0 V at sweep rate of 20 mV/s.

3. Results and discussions

3.1 ALD growth of NTO thin films

To optimize the NTO thin film properties, it is essential to understand the mechanism of Nb incorporation in SnO_2 by following the surface reactivity that occurred during the film growth. This can be elucidated by in-situ QCM measurement, which recorded mass variations occurring during the deposition process. Figure SI.1a-d shows the mass variations measured during the deposition of SnO_2, Nb_2O_5, SONO(10:1) and OSNO(10:1) thin films for several cycles. They all demonstrated a linear growth over time, which is a typical signature of ALD process [18,27]. The mass variations measured over one cycle for the two sequences are presented in Figure 1 and compared to the ones of pure SnO_2 and Nb_2O_5 thin films.

In the case of SnO_2 (Figure 1a), a positive mass variation ($\Delta m_1^{SnO_2}$ = 1.17 a.u.) was recorded after the pulse of TDMASn and a slight negative mass variation ($\Delta m_2^{SnO_2}$ = -0.01 a.u.) after the pulse of H_2O_2. These evolution values were in accordance with the reported ones of SnO_2 deposited from TDMASn and H_2O_2 at 150 °C, and imply that after TDMASn pulse about 80% of the DMA ligands were released while about 20% remained on the surface [19]. In the case of Nb_2O_5 thin films (Figure 1b), a positive mass variation ($\Delta m_1^{Nb_2O_5}$ = 0.58 a.u.) is recorded during the pulse of TBTDEN whereas a negative mass variation ($\Delta m_2^{Nb_2O_5}$ = -0.30 a.u.) is observed during the pulse of H_2O. These values are similar to the ones reported by Tomczak *et al* and indicate that one diethylamine is released upon TBTDEN pulse [32] (see details in Supporting Information).

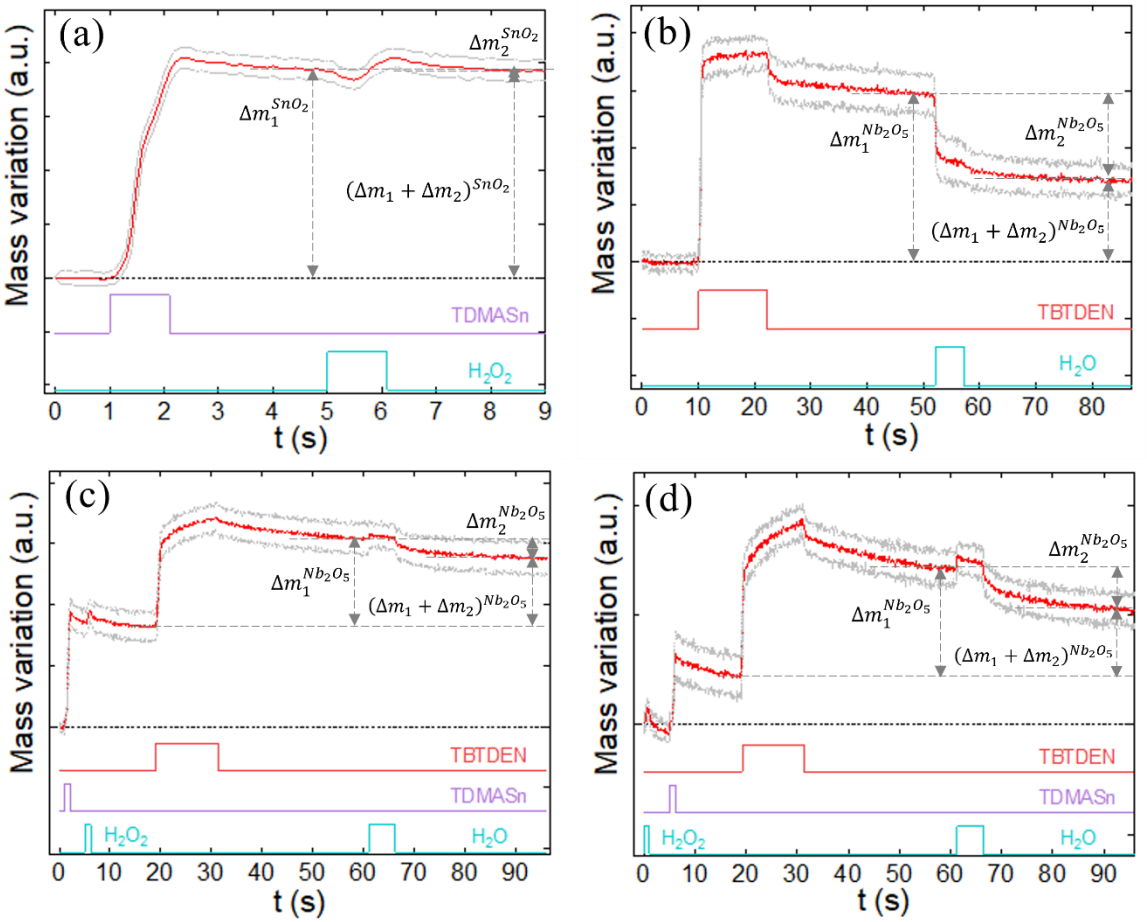

Figure 1. Mass variations recorded by in-situ QCM measurements for (a) SnO_2, (b) Nb_2O_5, Nb incorporation in (c) SONO(10:1), and (d) OSNO(10:1). The pulse times are depicted by bands below the curves.

As the order of precursor introduction is known to impact the surface reactions and the properties of the film [29–31], the mass variations during the incorporation of a single cycle of Nb_2O_5 into the SnO_2 cycles were also recorded. Figure 1c and 1d illustrated the mass variation during the incorporation of Nb_2O_5 in SONO(10:1), where the TBTDEN pulse is intercalated between a H_2O_2 and a H_2O pulse; and in OSNO(10:1) where the TBTDEN pulse is intercalated between a TDMASn and a H_2O pulse. Mass evolutions similar to the one where Nb_2O_5 grown on itself (Nb_2O_5) are measured, i.e. a positive mass variation ($\Delta m_1^{Nb_2O_5}$) during the pulse of TBTDEN and a negative one during the pulse of H_2O ($\Delta m_2^{Nb_2O_5}$) (Figure 1c,d). The obtained mass variation values during the growth of Nb_2O_5 on itself, in SONO(10:1), and in OSNO(10:1) sequences, are summarized in Table 1.

Table 1. Average mass variations of 10 cycles during the growth of Nb_2O_5: on itself, in SONO(10:1), and in OSNO(10:1) sequences.

	Nb_2O_5 grows		
Mass variation	on itself	SONO(10:1)	OSNO(10:1)
$\Delta m_1^{Nb_2O_5}$	0.58 ±0.05	0.72 ±0.05	0.49 ±0.05
$\Delta m_2^{Nb_2O_5}$	-0.30 ±0.05	-0.16 ±0.05	-0.19 ±0.05

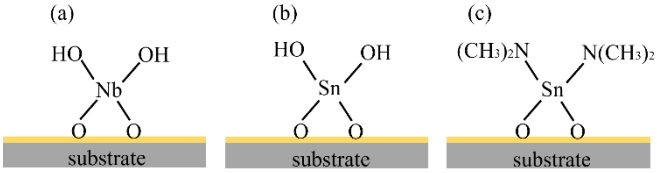

Figure 2. Schematic representation of the surface nature where Nb_2O_5 grows on (a) itself (Nb-OH surface), (b) SONO sequence (Sn-OH surface), and (c) OSNO sequence (Sn-DMA surface).

As shown in Table 1, the mass variations are different, which demonstrates that the growth of Nb_2O_5 is highly impacted by the surface nature. A schematic representation of the various nature of reactive surfaces during the TBTDEN pulse in Nb_2O_5 (Nb-OH), SONO (Sn-OH) and OSNO (Sn-DMA) are illustrated in Figure 2a-c. Such differences induce different reaction pathways with TBTDEN, as evidenced by the different mass variations. In case of SONO, although a -OH surface similar to the one of pure Nb_2O_5 is expected, the larger $\Delta m_1^{Nb_2O_5}$ values indicate that additional phenomena must be taken into account to discuss the growth mechanism. For instance, this can originate from different surface densities of –OH species. Indeed, considering the lower reactivity of H_2O vs H_2O_2, a larger amount of ligand may be exchanged during the pulse of TBTDEN on the Sn-OH surface (SONO) than on the Nb-OH surface (Nb_2O_5). On the other hand, the positive $\Delta m_1^{Nb_2O_5}$ value in OSNO indicates the incorporation of Nb containing fragments, even on Sn-DMA surface. The relative lower value can be attributed to the higher reactivity of TBTDEN towards Sn-OH surface species than Sn-DMA surface. The mass variation in OSNO can be attributed to the TBTDEN reacting with the Sn-DMA terminated groups or/and with the remaining Sn-OH surface species, or/and possible ligand sticking, or/and physisorption of the precursor. Those phenomena have already been observed for other ALD materials [28–30,33]. Additional characterizations, such as Residual Gas Analysis for etching mechanisms or XPS surface analysis to quantify the Nb incorporation level and identify potential molecule sticking are required to discriminate them.

3.2 Properties of NTO thin films

NTO thin films were fabricated using variable cycle ratios (SnO_2:Nb_2O_5 = 55:1, 20:1, 15:1, 10:1, 5:1, 1:1) and pulse sequences (SONO, OSNO). The thicknesses determined by ellipsometry and XRR are displayed in Figure SI.2 with values ranging between 15 and 20 nm. Film thickness homogeneity was confirmed over the whole substrate area (15x15 cm^2) regardless of the deposition conditions. The growth per cycle (GPC), determined by dividing the measured thickness by the total cycle number, of SnO_2 was found to be 1.50 Å/cycle in accordance with the reported one of 1.20 Å/cycle grown between 100-200 °C from TDMASn and H_2O_2 [19,34]. Nb_2O_5 thin films have a GPC of 0.80 Å/cycle, while it has been reported in the range of 0.38-0.2 Å/cycle deposited at 150-350 °C from TBTDEN and H_2O [35,36]. Thus, the obtained higher GPC in this work can be due to relatively lower deposition temperature. As shown in Figure SI.2, the measured thicknesses of NTO thin films are higher than the one that can be expected by the rule of mixture, i.e. combining the GPC of SnO_2 and Nb_2O_5 with the total number of cycles for each. This indicates that Nb incorporation involves a different growth mechanism than the individual components and confirms our QCM observations.

Structurally, all films appeared amorphous (Figure SI.3) regardless of deposition conditions, most likely due to low temperature (100 °C) and thickness. The fabricated thin films show a smooth surface as observed by cross-sectional SEM image (Figure SI.5b, Figure SI.6) and a roughness smaller than 0.5 nm (determined from XRR data, Figure SI.4). The XRR spectra shows that the critical angle (θ_c) of thin films consisting Nb slightly modified compared to SnO_2 thin films. This suggested the density of SnO_2 thin film has slightly changed with Nb atom incorporation. The density of SnO_2 thin films (Figure SI.5a) was found to be 5.61 g/cm^3 similar to the reported one [37], which is about 80% of the bulk crystalline value of SnO_2 (6.99 g/cm^3) [4]. The lower density can be associated to the amorphous structure of the thin films and/or

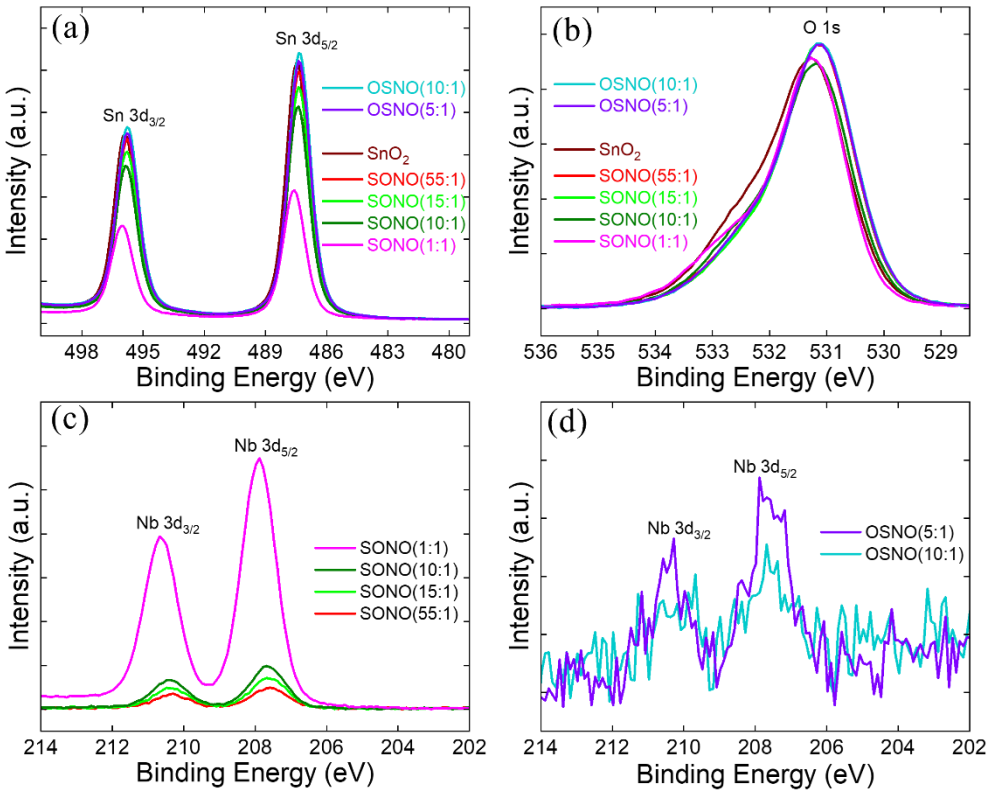

Figure 3. Normalized high-resolution XPS core level spectra of (a) Sn 3d, (b) O 1s, (c) Nb 3d (SONO sequence), (d) Nb 3d (OSNO) sequence.

presence of residual –OH groups [38]. Nb_2O_5 thin films have a density of 4.67 g/cm^3 in accordance with reported one of 4.36-5.12 g/cm^3 for the amorphous phase [39]. The incorporation of Nb highly modifies the density of SnO_2, which increases up to 6.4 g/cm^3 for SONO(15:1) while decreases up to 5.0 g/cm^3 for SONO(1:1) samples as shown in (Figure SI.5a). In almost all cases the measured densities of NTO thin films are different from the one expected by the rule of mixture, which may indicate the homogeneous distribution of Nb in the host SnO_2 matrix.

The incorporation level of Nb atom and chemical fine structure of the thin films were determined by XPS measurements by first collecting high-resolution spectra at the surface of the deposited films. It is important to note that the XPS probed depth is in the 10 nm range, which means that the collected information is representative of more than half of the layer. Figure 3 displays the high-resolution XPS spectra of Sn 3d, O1s and Nb 3d of the thin films of various cycle ratio and sequences. As shown in Figure 3a, all the Sn-containing films present the representative doublet peaks of Sn 3d at binding energy (BE +/- 0.3 eV) of 487.3 eV (Sn $3d_{5/2}$) and 495.7 eV (Sn $3d_{3/2}$) associated to the oxidation state of Sn^{+IV} [37]. No other oxidation states such as Sn^{+II} (Sn 3d $_{5/2}$ at 486.0 eV) [40] and Sn^0 (Sn 3d $_{5/2}$ at 484.7 eV) [41] were detected in the film,

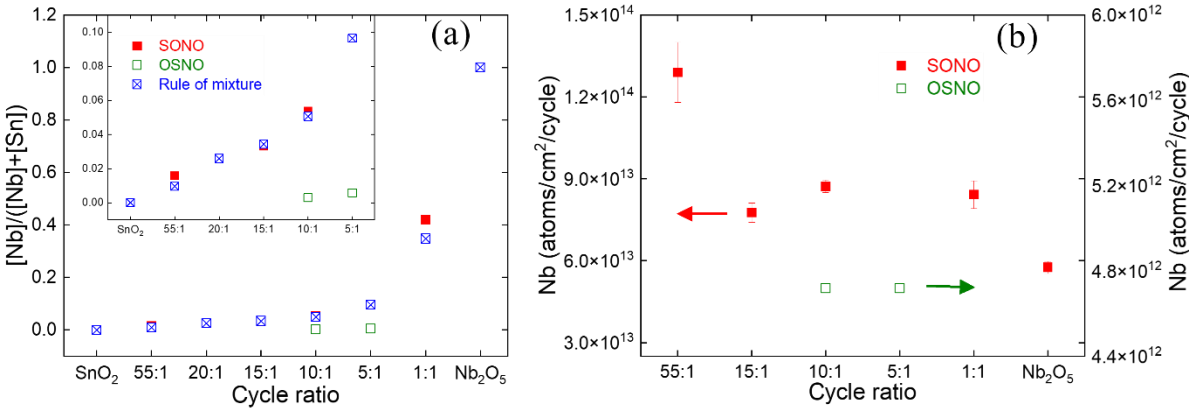

Figure 4. (a) Nb fraction [Nb]/([Nb]+[Sn]) determined by depth profile XPS, and by rule of mixture using the GPC of pure SnO_2 and Nb_2O_5 and their cycle ratio, (b) number of Nb atoms incorporated in one ALD cycle.

in agreement with the constancy of the FWHM at 1.3 eV in favour of a unique chemical environment. The XPS signature of O 1s (Figure 3b) presents a major peak at BE (+/- 0.3 eV) of 531.5 eV and a shoulder at 532.5 eV (Figure SI.7), that are ascribed to the different chemical environment of oxygen assigned to O-Sn^{+IV} bond and to the surface O-H, O-C, and C-C groups (adventitious carbon contamination), respectively. Figure 3c and 3d displays the XPS spectrum of Nb 3d in SONO and OSNO sequences, respectively, at BE of 207.5 eV (Nb $3d_{5/2}$) and 210.5 eV (Nb $3d_{3/2}$) attributed to the oxidation states of Nb^{+V} [42]. Intensity of Nb 3d peak increases as the SnO_2:Nb_2O_5 cycle ratio decreases (and reversely decrease for Sn 3d), which highlights that the Nb concentration increases inside the film. The compositions were determined from high-resolution spectra, without deconvolution of the chemical environments, but after two short sequences of Ar^+ sputtering (20 and 40 s) to get rid of the adventitious contamination and determine the variation of the atomic percentages of elements (Sn, Nb, O, C, and N) in the bulk. Ar^+ sputtering led as expected to preferential sputtering, leading to metal reduction by preferential O loss and thus preventing a reliable diagnosis of the O species but not to satisfactorily determine the ratio between the metallic elements. The Sn and Nb at.% inside the thin films (average of 20 and 40 s etching by sputtering) are presented in Table 2 and the fraction (Nb_F) was calculated as;

$$\mathbf{Nb_F} = \frac{[\mathbf{Nb}]}{[\mathbf{Nb}]+[\mathbf{Sn}]} \qquad \text{Equation 1}$$

where, [Sn] and [Nb] are the atomic percentages of Nb and Sn atoms. Figure 4a presents the variation of Nb fraction as a function of SnO_2:Nb_2O_5 cycle ratios in the NTO thin films in the two sequences. The Nb fraction increases as the cycle ratio decreases and confirms the successful incorporation of Nb atom in the SnO_2 structure, in agreement with QCM. In case of SONO sequence, the Nb fraction shows a linear trend with the cycle ratio up to 5:1 (Figure 4a, inset) in accordance to the reported NTO films fabricated by ALD [11]. For the same cycle ratio, lower Nb fractions are obtained by OSNO than SONO sequences, in agreement with the QCM result shown for OSNO(10:1) and SONO(10:1). The expected Nb fraction in the thin film can be calculated by rule of mixture [43] using the GPC of pure SnO_2 and Nb_2O_5, and their cycle ratio in the NTO thin film (equation 2).

$$\textbf{Rule of mixture} = \frac{\mathbf{GPC_{Nb_2O_5}}}{\mathbf{GPC_{Nb_2O_5}} + \mathbf{GPC_{SNO_2}} \cdot \mathbf{x1}} \qquad \text{Equation 2}$$

where, $GPC_{Nb_2O_5}$ and GPC_{SNO_2} are the growth per cycle for pure Nb_2O_5 and SnO_2, respectively, and x1 is the number of SnO_2 cycles in one supercycle. As shown in Figure 4a, the Nb fraction in SONO sequence obtained by depth profile XPS follows the one obtained by the rule of mixtures, whereas the fraction in OSNO sequence does not follow the trend. The

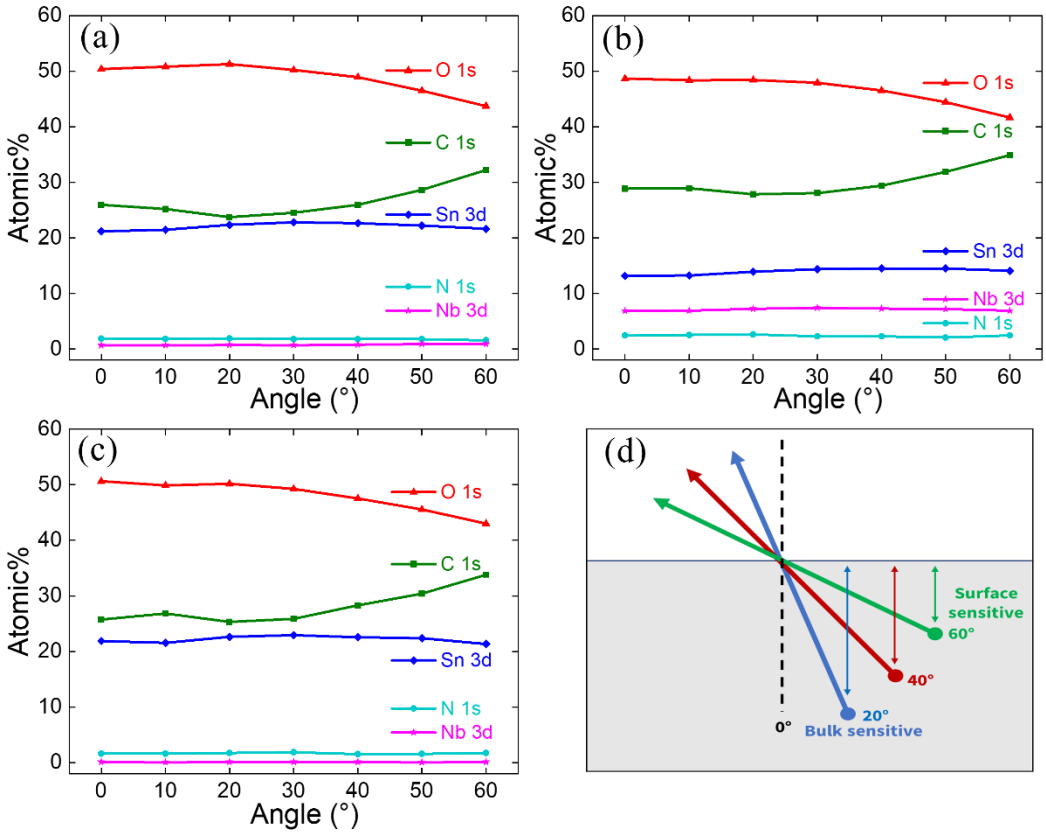

Figure 5. Elemental compositions in the NTO thin films collected by angle-resolved XPS measurements for (a) SONO(55:1), (b) SONO(1:1), (c) OSNO(10:1), (d) schematic representation of the correspondence between the measurement angle and the probed depth

latter is most likely due to the different nature of the surface Sn-DMA (Figure 2c), which impacted the growth mechanism that leads the Nb atomic fraction not to follow the principle of rule of mixture.

The effect of cycle ratios and precursor pulse sequences on the number of Nb atoms incorporated in one ALD cycle were evaluated using equation 3.

$$\boldsymbol{Nb_{NTO} = Nb_{Nb_2O_5}\, x\, \frac{Nb_2O_5\ cycles}{Nb_2O_5\ cycles_{NTO}} x \frac{\%Nb_{NTO}}{\%Nb_{Nb_2O_5}}} \quad \text{Equation 3}$$

where, $Nb_{Nb_2O_5}$ and Nb_{NTO} are the number of Nb atoms in 1 ALD cycle for pure Nb_2O_5 and NTO thin films, $Nb_2O_5\ cycles$ and $Nb_2O_5\ cycles_{NTO}$ are the total number of Nb_2O_5 ALD cycles in pure Nb_2O_5 and NTO thin film, $\%Nb_{Nb_2O_5}$ and $\%Nb_{NTO}$ are the Nb atomic percentage (Table 2) in pure Nb_2O_5 and NTO thin films determined by XPS depth profiles, respectively.

The $Nb_{Nb_2O_5}$ (5.76×10^{13} atom/cm^2/cycle) can be estimated using the density, GPC, and atomic percentage of Nb in the pure Nb_2O_5 thin films. Figure 4b shows the evolution of the average number of Nb atoms incorporated in one ALD cycle as a function of cycle ratios for the two sequences. As seen, the SONO(55:1) presents a higher Nb atoms incorporation per cycle which dropped in case of SONO(15:1) and then the variation decreases with cycle ratios. With the exception of SONO(1:1), all the SONO sequences inserted higher Nb atoms per cycle than the one in pure Nb_2O_5 whereas lower Nb atoms incorporated in OSNO sequences. Moreover, with the same cycle ratio, the OSNO sequences incorporated less Nb atoms than the corresponding SONO sequences. These results are consistent with the QCM observation (Figure 1 and Table 1), which shows a higher mass variation ($\Delta m_1^{Nb_2O_5}$) during the pulse of TBTDEN in SONO(10:1) sequence than OSNO(10:1) sequences and the one grown on itself.

As the fabricated films are thin enough ($\leq$ 20nm), the distribution of elements can be investigated using angle-resolved XPS (ARXPS), tilting the samples from 0° to 60° without etching, as shown in Figure 5d. It enables refining the chemical diagnosis within the initial 10 nm probed when operating at normal incidence (0° angle). Figure 5(a-c) illustrates the elemental atomic percentage of Sn, Nb, O, C, and N in the SONO(55:1), SONO(1:1), and OSNO(10:1) samples collected at different angles. A similar atomic percentage of Sn and Nb are probed for 0-30° angles for a given sample that confirm the homogeneous distribution of the elements at the surface and sub-surface at the XPS resolution scale. For higher angles, the surface sensitivity increases and higher contents of C are detected for all samples, linked to air contamination. Inside the thin film it is less than 5% as determined by Ar+ depth profile analyses (see composition details in Table SI.1). Indeed, this low content of C but also N atoms (< 2 at.%), show that a very low amount of precursors residues are incorporated inside the thin films confirming the good reactivities of Sn and Nb precursors during ALD process. Furthermore, this very low C and N contents disprove the hypothetical physisorption of the precursor or/and ligand sticking to account for the recorded positive mass variations during the pulse of TBTDEN in OSNO(10:1) sequence (Figure 1d). It rather shows that it is most likely due to the TBTDEN reacts with the Sn-DMA surface or/and the remaining -OH groups.

The optical features of the thin films were analyzed by measuring their transmission and reflectivity (Figure SI.8) for thin films grown on borosilicate glass. The SnO_2, Nb_2O_5, and NTO thin films are very transparent in the visible and infrared range of 600-2500 nm with transmittance value greater than 90% and reflectivity less than 15%. In this spectrum range both the variation of cycle ratio and precursor pulse sequences do not show a significant effect on the transparency and reflectivity of thin films, possibly due to their closer thickness (15-20 nm). The transmittance slightly decreases in the range of 300-600 nm with intrinsic effects where the thin film absorbs light. The transmittance in this work is higher than the reported one of NTO thin films obtained by spin coating regarding the 20 nm thickness [44].

To account for various potential applications, the transmittance efficiency ($E_{T(\lambda)}^{AM1.5}$) of the reference solar spectral irradiance AM1.5 global by the thin films transmittance was evaluated over a wide spectral range (300-1000 nm), as proposed elsewhere [45] (details in SI). The calculated $E_{T(\lambda)}^{AM1.5}$ were found that all the thin films transmits more than 96% of the AM1.5 global solar irradiance. This makes the thin films suitable for various optoelectronic and photovoltaic devices, for instance as transparent conductive oxide and electron transport layer.

The optical band gap energy (E_g) were determined from the transmission and reflectivity, considering direct transition of SnO_2 and NTO thin films while indirect transition for Nb_2O_5, using Tauc plot [46]. The E_g values are illustrated in Figure 6, for SnO_2 (3.80 eV) and Nb_2O_5 (3.45 eV) thin films similar to the reported one [47] and [36], respectively. In case of NTO thin films (SONO sequence), initially the E_g slightly increases possibly due to Moss-Burstein effect [48] and then dropped

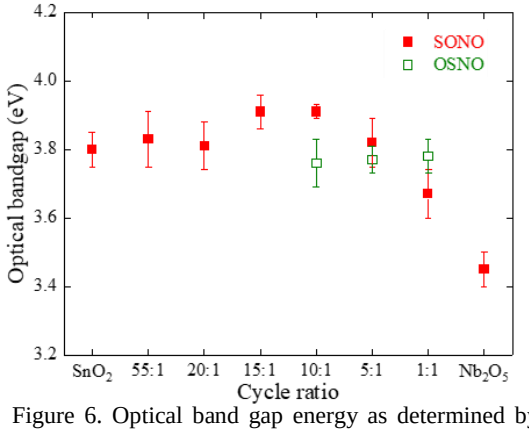

Figure 6. Optical band gap energy as determined by Tauc formalism, of thin films with SONO and OSNO sequences at various cycle ratio

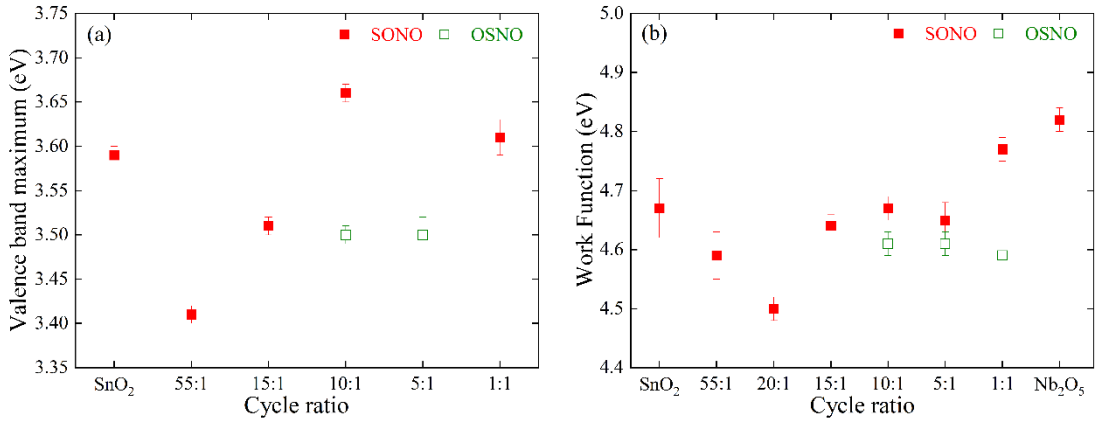

Figure 7. (a) Valence band maximum, and (b) work function, of the NTO thin films as determined by XPS spectra at low BE and Kelvin Probe respectively.

down that can be due to defect sites introduced as the Nb content increase, in accordance with other reports [10] [49]. For thin films in OSNO sequences, the decrease in E_g value compared to pure SnO_2 (Figure 6) may not be explained by either the Moss-Burstein effect or by the introduction of defect sites since the Nb concentration is low ($\leq$ 0.2 at.%). Rather, this might be most likely ascribed to the substitution of Nb^{+V} ions that introduce electron states in the band structure of SnO_2 to form a new lowest unoccupied molecular orbital [50].

The XPS spectra at low BE region (Figure SI.9a) showed that the incorporation of Nb modifies the top edge position of valence band of SnO_2 (Figure 7a). The valence band maximum (E_{VB}) of SnO_2 (3.6 eV) is shifted to either lower values for SONO(55:1), SONO(15:1), OSNO(10:1), and OSNO(5:1) or to higher values for SONO(10:1), SONO(1:1). Moreover, the work function (Φ) of the thin films, which is associated to the Fermi level (E_F) position of vacuum level, E_{vac}, i.e., $\Phi = E_{vac} - E_F$, were also evaluated (Figure 7b). The work function of pure SnO_2 thin film was found to be 4.7 eV which is in the range of the reported value of 4.4-5.7 eV by RF magnetron sputtered SnO_2 thin film [51]. With the exception of SONO(1:1), the Nb incorporated SnO_2 thin film have a lower Φ compared to the pure SnO_2 thin film. This indicates that the E_F level is shifted towards the conduction band [52], which is consistent to the evolution of the calculated conduction band minimum ($E_{CBM} = E_{VBM} - E_g$) (see SI). Both the conduction band minimum and valence band maximum of NTO thin films, which involves $\leq$ 1 at.% of Nb, shifted down to lower value compared to the undoped SnO_2, in accordance with the reported theoretical study [53].

Electrical parameters (bulk concentration, resistivity, and mobility) of thin films obtained by Hall measurement are illustrated in Table 2. The Hall parameters of pure SnO_2 and Nb_2O_5 and several other NTO thin films could not be determined due to their too resistive nature. Among the fabricated NTO thin films, SONO(55:1), SONO(15:1), and OSNO(10:1) samples could be evaluated by Hall measurements, which shows that the incorporation of Nb atom tuned the electrical properties of SnO_2 from resistive to conductive nature. As seen in Table 2, thin films obtained by SONO sequences show conductive nature for thin films containing lower concentration of Nb ($\leq$1.15 at.%). The enhanced electrical parameters, for Nb $\leq$1.15 at.%, can be explained by the substitutional incorporation of Nb^{+V} ions at Sn^{+IV} cation site where Nb atoms act as electron donor leading to increase the carrier concentration and decreases the resistivity [9,14]. The negative sign in the bulk concentration of the conductive films (Table 2) indicates that electrons are the majority carriers (*n*-type semiconductor), which was further confirmed by cyclic voltammograms (CV) (Figure SI.10) for all thin films. Moreover, the CV shows that all the fabricated thin films (thickness 15-20 nm) have the hole-blocking ability that paves the way toward the integration of this layer in optoelectronic and photovoltaic devices. As the Nb concentration increases more than 1.15 at.%, the electrical parameters could not be determined by Hall measurements. This can be ascribed to the excess amount of Nb^{+V} ions may increase the defects (e.g. ionized impurities, interstitial atoms), which can increases the carrier scattering leading to decrease of the electron mobility and films become resistive [10]. Similar evolutions of electrical parameters with Nb concentration have been observed in other studies on NTO thin films obtained by alternative methods [54] [9].

Table 2. Metallic ratio Nb/(Nb+Sn) (after 20-40s sputtering) and electrical parameters determined by Hall measurements of prepared thin films.

Sample name	Nb/ (Nb+Sn)	Bulk conc. (/cm^3)	Resistivity (Ω.cm)	Mobility (cm^2/V s)
SnO_2	0	*	*	*
SONO(55:1)	0.016	-2.5x10^{18}	3.17	0.7-0.8
SONO(15:1)	0.033	-(1-6)x10^{17}	31	0.2-2.2
SONO(10:1)	0.054	*	*	*

SONO(5:1)	--	*	*	*
SONO(1:1)	0.42	*	*	*
OSNO(10:1)	0.003	-(0.2-2.2)x10^{18}	22.3	0.12-1.26
OSNO(5:1)	0.006	*	*	*
OSNO(1:1)	--	*	*	*
Nb_2O_5	1.0	*	*	*

* indicates that the films were too resistive for Hall measurements.

Doping level and doping efficiency of functional material are important factors that can determine the performance of a device. In this study, the optimum Nb incorporation level was found to be about 1 at.% that is similar to the reported one by Suzuki et al [55] and Liu et al [44], whereas lower (0.5 at.%, [54]) and higher (1.94-2 at.% [11],[14]) values are also reported. Comparatively, the Hall parameters obtained in this work remain lower than the reported values. However, those correspond to as-deposited ultra-thin (<20 nm) films, deposited at 100 °C whereas reported ones are either produced at temperature higher than 200 °C or/and annealed at 400 °C and above [11,54,55]. The highest bulk concentration ($2.5x10^{18}/cm^3$, SONO(55:1)) obtained in this work, is in the same order of magnitude of NTO films containing 1 at.% of Nb synthesized by MOCVD at 600 °C [10].

This report also evidenced that electrical properties can be efficiently tuned by exchanging the precursor pulse sequences during the ALD process. As shown in Table 2, a more conductive thin films of OSNO(10:1) was obtained than the corresponding SONO(10:1). Unfortunately, the doping efficiency as proposed elsewhere [28] cannot be quantified due to the resistive nature of SnO_2 thin films, which is the reference to evaluate the effect of doping. However, by comparing the Nb at% and bulk concentration of the conductive thin films, i.e. SONO(55:1), SONO(15:1), and OSNO(10:1), one can predict that the OSNO sequence allows a higher doping efficiency.

This confirms the capability of the precursor pulse sequences to control the distribution of the incorporated atoms in the thin film [29–31] and demonstrates its applicability to generate efficient Nb-doped SnO_2 ultra-thin films at low temperature.

4. Conclusions

Conductive ultra-thin SnO_2 films have been successfully fabricated by ALD at low deposition temperature (100°C) by incorporating niobium atoms. Variation of cycle ratios and pulse sequences were found key-parameters to tune optoelectrical properties of SnO_2:Nb (NTO) thin films. A fine growth mechanism study based on in-situ QCM measurement and XPS spectra revealed that the Nb incorporation mechanism is highly impacted by both the chemical nature and the density of the surface species. Accordingly, the actual amount of Nb atoms inserted in the thin films were highly influenced by the pulse sequences.

Highly transparent thin films with transmittance greater than >90% in the visible and infrared range were generated. The incorporation of Nb modifies the band gap, valence and conduction bands of SnO_2. Depending on the supercycle ratio and precursor sequence, Nb content and distribution could be controlled. Consequently, the electrical properties of SnO_2 could be tuned from resistive to conductive nature. In this work, optimal incorporation level of Nb was found $\leq$1 at.% to obtain a conductive thin films. The high optical transparency accompanied with comparable electrical properties of NTO thin films fabricated at lower deposition temperature paves the way for the integration of these layers in temperature-sensitive, nanostructured optoelectronic devices.

Authors Contributions

Getaneh Diress Gesesse: Data curation, Formal analysis, Investigation, Visualization, Writing-original draft, Writing – review&editing.

Damien Coutancier : Data curation, Formal analysis, Investigation, Visualization, Writing – review&editing.

Mirella Al Katrib : Data curation, Formal analysis, Investigation, Writing – review&editing

Frédérique Donsanti: Writing – review&editing

Muriel Bouttemy : Supervision, Validation, Writing – review&editing.

Nathanaelle Schneider : Conceptualization, Funding acquisition, Project administration, Supervision, Validation, Writing – review&editing.

Acknowledgements

This project was supported by the French Government in the frame of the program of investment for the future (Programme d'Investissement d'Avenir - ANR-IEED-002-01). The authors would like to thank Alexandre Blaizot (IPVF) for SEM images.

References

[1] Dalapati G K, Sharma H, Guchhait A, Chakrabarty N, Bamola P, Liu Q, Saianand G, Sai Krishna A M, Mukhopadhyay S, Dey A, Wong T K S, Zhuk S, Ghosh S, Chakrabortty S, Mahata C, Biring S, Kumar A, Ribeiro C S, Ramakrishna S, Chakraborty A K, Krishnamurthy S, Sonar P and Sharma M 2021 Tin oxide for optoelectronic, photovoltaic and energy storage devices: a review *J. Mater. Chem. A* **9** 16621–84

[2] Xu Y, Zheng L, Yang C, Zheng W, Liu X and Zhang J 2020 Oxygen Vacancies Enabled Porous SnO2 Thin Films for Highly Sensitive Detection of Triethylamine at

Room Temperature *ACS Appl. Mater. Interfaces* **12** 20704–13

[3] Ji Y-C, Zhang H-X, Zhang X-H and Li Z-Q 2013 Structures, optical properties, and electrical transport processes of SnO2 films with oxygen deficiencies *physica status solidi (b)* **250** 2145–52

[4] Batzill M and Diebold U 2005 The surface and materials science of tin oxide *Progress in Surface Science* **79** 47–154

[5] Dubau L, Maillard F, Chatenet M, Cavaliere S, Jiménez-Morales I, Mosdale A and Mosdale R 2020 Durability of Alternative Metal Oxide Supports for Application at a Proton-Exchange Membrane Fuel Cell Cathode—Comparison of Antimony- and Niobium-Doped Tin Oxide *Energies* **13** 403

[6] Shannon R D 1976 Revised effective ionic radii and systematic studies of interatomic distances in halides and chalcogenides *Acta Crystallographica Section A* **32** 751–67

[7] Zainullina V M 2007 Electronic structure, chemical bonding and properties of Sn1−xMxO2, M=As, Sb, Bi, V, Nb, Ta (0.0⩽x⩽0.25) *Physica B: Condensed Matter* **391** 280–5

[8] Halvani Anaraki E, Kermanpur A, Mayer M T, Steier L, Ahmed T, Turren-Cruz S-H, Seo J, Luo J, Zakeeruddin S M, Tress W R, Edvinsson T, Grätzel M, Hagfeldt A and Correa-Baena J-P 2018 Low-Temperature Nb-Doped SnO_2 Electron-Selective Contact Yields over 20% Efficiency in Planar Perovskite Solar Cells *ACS Energy Lett.* **3** 773–8

[9] Seo Y J, Kim G W, Sung C H, Anwar M S, Lee C G and Koo B H 2011 Characterization of transparent and conductive electrodes of Nb-doped SnO2 thin film by pulsed laser deposition *Current Applied Physics* **11** S310–3

[10] He L, Luan C, Feng X, Xiao H and Ma J 2018 Effect of niobium doping on the structural, electrical and optical properties of epitaxial SnO2 films on MgF2 (110) substrates by MOCVD *Journal of Alloys and Compounds* **741** 677–81

[11] Stefik M, Cornuz M, Mathews N, Hisatomi T, Mhaisalkar S and Grätzel M 2012 Transparent, Conducting Nb:SnO_2 for Host–Guest Photoelectrochemistry *Nano Lett.* **12** 5431–5

[12] Zhang S, Zhang J, Cao G, Wang Q, Hu J, Zhang P and Shao G 2018 Strong interplay between dopant and SnO2 in amorphous transparent (Sn, Nb)O2 anode with high conductivity in electrochemical cycling *Journal of Alloys and Compounds* **735** 2401–9

[13] Wang S, Shen W, Liu J, Ouyang T, Wu Y, Li W, Chen M, Qi P, Lu Y and Tang Y 2021 Improved photovoltage of printable perovskite solar cells via Nb5+ doped SnO2 compact layer *Nanotechnology* **32** 145403

[14] Turgut G, Keskenler E F, Aydın S, Sönmez E, Doğan S, Düzgün B and Ertuğrul M 2013 Effect of Nb doping on structural, electrical and optical properties of spray deposited SnO2 thin films *Superlattices and Microstructures* **56** 107–16

[15] Wang Y, Brezesinski T, Antonietti M and Smarsly B 2009 Ordered Mesoporous Sb-, Nb-, and Ta-Doped SnO_2 Thin Films with Adjustable Doping Levels and High Electrical Conductivity *ACS Nano* **3** 1373–8

[16] Johnson R W, Hultqvist A and Bent S F 2014 A brief review of atomic layer deposition: from fundamentals to applications *Materials Today* **17** 236–46

[17] Leskelä M, Mattinen M and Ritala M 2019 Review Article: Atomic layer deposition of optoelectronic materials *Journal of Vacuum Science & Technology B, Nanotechnology and Microelectronics: Materials, Processing, Measurement, and Phenomena* **37** 030801

[18] George S M 2010 Atomic Layer Deposition: An Overview *Chem. Rev.* **110** 111–31

[19] Elam J W, Baker D A, Hryn A J, Martinson A B F, Pellin M J and Hupp J T 2008 Atomic layer deposition of tin oxide films using tetrakis(dimethylamino) tin *Journal of Vacuum Science & Technology A* **26** 244–52

[20] Pore V, Ritala M, Leskelä M, Saukkonen T and Järn M 2009 Explosive Crystallization in Atomic Layer Deposited Mixed Titanium Oxides *Crystal Growth & Design* **9** 2974–8

[21] Shaw A, Wrench J S, Jin J D, Whittles T J, Mitrovic I Z, Raja M, Dhanak V R, Chalker P R and Hall S 2016 Atomic layer deposition of Nb-doped ZnO for thin film transistors *Appl. Phys. Lett.* **109** 222103

[22] Blomberg T, Wenger Ch, Baristiran Kaynak C, Ruhl G and Baumann P 2011 ALD grown NbTaO based MIM capacitors *Microelectronic Engineering* **88** 2447–51

[23] Liu J, Xu Y, Sun Q, Lu H and Zhang D W 2011 Characterizations of NbAlO thin films grown by atomic layer deposition *Materials Letters* **65** 2182–4

[24] Lee S-H, Choi J-M, Lim J-H, Park J and Park J-S 2018 A study on the thermoelectric properties of ALD-grown aluminum-doped tin oxide with respect to nanostructure modulations *Ceramics International* **44** 1978–83

[25] Cho C J, Pyeon J J, Hwang C S, Kim J-S and Kim S K 2019 Atomic layer deposition of Ta-doped SnO2 films with enhanced dopant distribution for thermally stable capacitor electrode applications *Applied Surface Science* **497** 143804

[26] Hu Y, Yella A, Guldin S, Schreier M, Stellacci F, Grätzel M and Stefik M 2014 High-Surface-Area Porous Platinum Electrodes for Enhanced Charge Transfer *Adv. Energy Mater.* **4** 1400510

[27] Mackus A J M, Schneider J R, MacIsaac C, Baker J G and Bent S F 2019 Synthesis of Doped, Ternary, and Quaternary Materials by Atomic Layer Deposition: A Review *Chem. Mater.* **31** 1142–83

[28] Wu Y, Potts S E, Hermkens P M, Knoops H C M, Roozeboom F and Kessels W M M 2013 Enhanced Doping Efficiency of Al-Doped ZnO by Atomic Layer Deposition Using Dimethylaluminum Isopropoxide as an Alternative Aluminum Precursor *Chem. Mater.* **25** 4619–22

[29] Na J-S, Peng Q, Scarel G and Parsons G N 2009 Role of Gas Doping Sequence in Surface Reactions and Dopant Incorporation during Atomic Layer Deposition of Al-Doped ZnO *Chem. Mater.* **21** 5585–93

[30] Coutancier D, Zhang S-T, Bernardini S, Fournier O, Mathieu-Pennober T, Donsanti F, Tchernycheva M, Foldyna M and Schneider N 2020 ALD of ZnO:Ti: Growth Mechanism and Application as an Efficient Transparent Conductive Oxide in Silicon Nanowire Solar Cells *ACS Appl. Mater. Interfaces* **12** 21036–44

[31] Le Tulzo H, Schneider N, Lincot D, Patriarche G and Donsanti F 2018 Impact of the sequence of precursor introduction on the growth and properties of atomic layer deposited Al-doped ZnO films *Journal of Vacuum Science & Technology A: Vacuum, Surfaces, and Films* **36** 041502

[32] Tomczak Y, Knapas K, Sundberg M, Leskelä M and Ritala M 2012 In Situ Reaction Mechanism Studies on the New tBuN=M(NEt2)3 -Water and tBuN=M(NEt2)3 -Ozone (M = Nb,Ta) Atomic Layer Deposition Processes *Chem. Mater.* **24** 1555–61

[33] Elam J W, Sechrist Z A and George S M 2002 ZnO/Al2O3 nanolaminates fabricated by atomic layer deposition: growth and surface roughness measurements *Thin Solid Films* **414** 43–55

[34] Choi D, Maeng W J and Park J-S 2014 The conducting tin oxide thin films deposited via atomic layer deposition using Tetrakis-dimethylamino tin and peroxide for transparent flexible electronics *Applied Surface Science* **313** 585–90

[35] Blanquart T, Niinistö J, Heikkilä M, Sajavaara T, Kukli K, Puukilainen E, Xu C, Hunks W, Ritala M and Leskelä M 2012 Evaluation and Comparison of Novel Precursors for Atomic Layer Deposition of Nb_2O_5 Thin Films *Chem. Mater.* **24** 975–80

[36] Basuvalingam S B, Macco B, Knoops H C M, Melskens J, Kessels W M M (Erwin) and Bol A A 2018 Comparison of thermal and plasma-enhanced atomic layer deposition of niobium oxide thin films *Journal of Vacuum Science & Technology A* **36** 041503

[37] Heo J, Hock A S and Gordon R G 2010 Low Temperature Atomic Layer Deposition of Tin Oxide *Chem. Mater.* **22** 4964–73

[38] Larsson F, Keller J, Primetzhofer D, Riekehr L, Edoff M and Törndahl T 2019 Atomic layer deposition of amorphous tin-gallium oxide films *Journal of Vacuum Science & Technology A: Vacuum, Surfaces, and Films* **37** 030906

[39] Schäfer H, Gruehn R and Schulte F 1966 The Modifications of Niobium Pentoxide *Angew. Chem. Int. Ed. Engl.* **5** 40–52

[40] Sun Q, Diao K, Sun T, Li M, Cui X, Tian H and Xiang B 2016 Enhanced gas-sensing performance of SnO2/Nb2O5 hybrid nanowires *RSC Adv.* **6** 105317–21

[41] Kakinuma K, Suda K, Kobayashi R, Tano T, Arata C, Amemiya I, Watanabe S, Matsumoto M, Imai H, Iiyama A and Uchida M 2019 Electronic States and Transport Phenomena of Pt Nanoparticle Catalysts Supported on Nb-Doped SnO2 for Polymer Electrolyte Fuel Cells *ACS Appl. Mater. Interfaces* **11** 34957–63

[42] Hoffeditz W L, Pellin M J, Farha O K and Hupp J T 2017 Determining the Conduction Band-Edge Potential of Solar-Cell-Relevant Nb_2O_5 Fabricated by Atomic Layer Deposition *Langmuir* **33** 9298–306

[43] Wu Y, Hermkens P M, Van De Loo B W H, Knoops H C M, Potts S E, Verheijen M A, Roozeboom F and Kessels W M M 2013 Electrical transport and Al doping efficiency in nanoscale ZnO films prepared by atomic layer deposition *Journal of Applied Physics* **114** 024308

[44] Liu J, Li N, Dong Q, Li J, Qin C and Wang L 2019 Tailoring electrical property of the low-temperature processed SnO2 for high-performance perovskite solar cells *Sci. China Mater.* **62** 173–80

[45] Boileau A, Hurand S, Baudouin F, Lüders U, Dallocchio M, Bérini B, Cheikh A, David A, Paumier F, Girardeau T, Marie P, Labbé C, Cardin J, Aureau D, Frégnaux M, Guilloux-Viry M, Prellier W, Dumont Y,

Demange V and Fouchet A 2022 Highly Transparent and Conductive Indium-Free Vanadates Crystallized at Reduced Temperature on Glass Using a 2D Transparent Nanosheet Seed Layer *Adv Funct Materials* **32** 2108047

[46] Tauc J, Grigorovici R and Vancu A 1966 Optical Properties and Electronic Structure of Amorphous Germanium *Physica Status Solidi (b)* **15** 627–37

[47] Guo R, Zhao Y, Zhang Y, Deng Q, Shen Y, Zhang W and Shao G 2021 Significant performance enhancement of all-inorganic CsPbBr3 perovskite solar cells enabled by Nb-doped SnO2 as effective electron transport layer *ENERGY & ENVIRONMENTAL MATERIALS* **4** 671–80

[48] Burstein E 1954 Anomalous Optical Absorption Limit in InSb *Phys. Rev.* **93** 632-633.

[49] Ramarajan R 2019 Thermal stability study of niobium doped SnO2 thin film for transparent conducting oxide application *Superlattices and Microstructures* **135** 106274

[50] Chandran D, NAIR L S, BALACHANDRAN S, BABU K R and DEEPA M 2016 Band gap narrowing and photocatalytic studies of Nd3+ ion-doped SnO2 nanoparticles using solar energy *Bull Mater Sci* **39** 27–33

[51] Klein A, Körber C, Wachau A, Säuberlich F, Gassenbauer Y, Schafranek R, Harvey S P and Mason T O 2009 Surface potentials of magnetron sputtered transparent conducting oxides *Thin Solid Films* **518** 1197–203

[52] Ramarajan R, Kovendhan M, Thangaraju K and Joseph D P 2020 Indium-free large area Nb-doped SnO2 thin film as an alternative transparent conducting electrode *Ceramics International* **46** 12224–31

[53] Cheng D, Zhang M, Chen J, Yang C, Zeng X and Cao D 2014 Computer Screening of Dopants for the Development of New SnO_2 -Based Transparent Conducting Oxides *J. Phys. Chem. C* **118** 2037–43

[54] Gokulakrishnan V, Parthiban S, Jeganathan K and Ramamurthi K 2011 Investigations on the structural, optical and electrical properties of Nb-doped SnO2 thin films *J Mater Sci* **46** 5553–8

[55] Suzuki A Y, Nose K, Ueno A, Kamiko M and Mitsuda Y 2012 High Transparency and Electrical Conductivity of SnO$_{2}$:Nb Thin Films Formed through (001)-Oriented SnO:Nb on Glass Substrate *Appl. Phys. Express* **5** 011103